Pergamon

Int. J. Heat Mass Transfer. Vol. 38, No. 18, pp. 3401–3412, 1995

0017-9310/95 $9.50+0.00

0017-9310(95)00075-5

A theoretical study of the transient coupled conduction and radiation heat transfer in glass: phonic diffusivity measurements by the flash technique

S. ANDRE and A. DEGIOVANNI

L.E.M.T.A CNRS URA 875, B.P. 160, 2 Av. de la Forêt de Haye, 54504 Vandoeuvre-lés-Nancy Cedex, France

(*Received* 24 *December* 1993 *and in final form* 15 *February* 1995)

Abstract—Evaluating the phonic conductivity of glasses is difficult because of the combined mode of heat transfer. In this work, a model is developed for the flash experiment, and numerical results are reported. Simulations in the non-gray case have shown that heat transfer in the sample is completely free from any radiative contribution for conditions of small optical thicknesses and reflecting walls. Thus diffusivity identified from the rear-face thermogram is a quantity of phonic origin. Experimental values for phonic conductivity are presented. The results for float glass are in agreement with literature data. For silica, a new result has been obtained: the temperature dependence of the phonic conductivity is found to be similar to that of its specific heat, confirming microscopic models of thermal conductivity in disordered systems.

1. INTRODUCTION

In the conception of a metrological process for the thermal characterization of semi-transparent materials (STMs), the combined conductive–radiative heat transfer problem must be considered. This problem can be treated accurately with an energy model if four intrinsic properties can be pre-defined: (1) the true phonic diffusivity (conductivity); (2) the true specific heat capacity; (3) the spectral absorption coefficient; (4) the index of refraction components. Among these parameters, the phonic diffusivity is far from the simplest to measure and the lack of data on this parameter can explain the efforts made by researchers in this field during the past two decades.

The needs for a precise knowledge of this quantity are numerous in engineering sciences. For example, predicting thermal behavior during glass making or forming processes, estimating the insulation properties at high temperatures, controlling industrial processes that involve fused quartz (production of optical fibers or in the semiconductor industry). Such progress can also lead to a better understanding of the phonon–phonon interaction in disordered systems through comparison of reliable data for the phonic conductivity of various glasses at high temperatures with the predictions of microscopic approaches.

In the case of the flash method, the transient coupled problem has to be solved. The non-steady case for an absorbing and emitting medium has been widely studied since 1970 [1–4] for various radiative boundary conditions. In 1975, Viskanta and Anderson [5] reviewed the literature available on the subject. The reported studies dealt mainly with prescribed temperature conditions at the boundaries of the system. Saulnier [6] improved and developed a nodal analysis based on the zoning method of Hottel and Sarofim [7]: it allowed extensive numerical calculations of temperature fields in the transient state for a system irradiated by a heat pulse on one of its black frontiers. This led Tan and Lallemand [8] to extend the previous problem to all kinds of convective–radiative heat exchanges at the boundaries. Finally, Tan *et al.* [9] considered a radiative external pulse, or an irradiation step, to simulate what happens in the flash technique. They concluded that it was possible to use the response of an STM to identify thermal diffusivities by a flash technique but pointed out that a well-adapted model was necessary in order to precisely define which diffusivity is obtained, and under which conditions. This is the aim of the current work.

The study described here consists in developing a theoretical model of a one-dimensional transient combined heat transfer for the different thermal responses associated with different experimental conditions. The model has been developed keeping in mind that the known parameters are the thickness of the sample, the type of glass, the radiative limits and the temperature level (300–800 K for our metrological set-up). The model is described in Section 2, and a finite-difference scheme is used to solve the energy equation. Coupling with the radiative transfer equation (RTE) is achieved through a source term which depends on the divergence of the radiative flux. This latter is obtained in a semi-analytical manner from the solution of the RTE. The non-gray character of various glasses can then be taken into account by simply computing the radiative

NOMENCLATURE

a_{ph} $k_{ph}/(\rho C_p)$ = phonic diffusivity [$m^2\ s^{-1}$]
Bi_1, Bi_2 Biot number at $z^* = 0$, $(h_1 e/k_{ph})$ and $z^* = 1$, $(h_2 e/k_{ph})$
C_p specific heat [$J\ kg^{-1}\ K^{-1}$]
e thickness of the slab [m]
E_i exponential integral function of order i
$F_{0-\lambda T}$ fraction of total blackbody intensity in 0–λT region
h_1, h_2 heat transfer coefficient at $z^* = 0$ and $z^* = 1$ respectively [$W\ m^{-2}\ K^{-1}$]
k thermal conductivity [$W\ m^{-1}\ K^{-1}$]
k^* k_{app}/k_{ph}, dimensionless conductivity
L intensity, radiant energy
L_m^* $\pi L_m/(4n_m^2\sigma T_0^4)$, dimensionless intensity
$L^\circ(T)$ blackbody intensity at temperature T
NB total number of spectral bands
NM total number of volumes
N_m $k_{ph}\chi_m/(4n_m^2\sigma T_0^3)$, gray Planck number
n refractive index
p non-linear diffusion coefficient
q_c conductive heat flux [$W\ m^{-2}$]
q_r radiative heat flux [$W\ m^{-2}$]
$q_{r_m}^*$ $q_{r_m}/(4n_m^2\sigma T_0^4)$, dimensionless radiative flux
Q heat pulse surface density [$J\ m^{-2}$]
s source term function
t physical time [s]
t^* $a_{ph}t/e^2$, dimensionless time
T temperature [K]
T_0 reference temperature [K]
z space variable [m].

Greek symbols
ε_1, ε_2 total emissivity of surfaces 1 and 2
θ^* $T^* - T_0^* = (T - T_0)/(Q/\rho C_p e)$, dimensionless temperature
λ wavelength [m]
μ directional cosine between z and L
ρ density [$kg\ m^{-3}$]
ρ_1, ρ_2 total reflectivity of surfaces 1 and 2
σ Stefan–Boltzmann constant
τ_{0m} $\chi_m e$ = gray optical thickness
χ absorption coefficient [m^{-1}].

Superscripts
* refers to dimensionless quantities.

Subscripts
λ refers to a spectral dependence
m refers to a spectral band
ph phonic quantity
r radiative quantity.

heat flux on rectangular spectral bands. In Section 3, we present experimental thermograms that point out interesting features of the physics governing the transient heat transfer. The conditions for the existence of a heat transfer equivalent to the purely conductive case are discussed. Then, the influence of the thickness of the slab on the identified diffusivity is studied for a given glass. It can be shown that conditions exist for which the estimated parameter is independent of the thickness (a very sensitive parameter for radiative transfer). This shows that the flash method can lead to direct measurement of the phonic diffusivity of semi-transparent materials. It is shown in Section 3 that the spectral dependence of the absorption coefficient of the glass does not modify the conclusions found in the gray case as long as the experimental conditions ensure that bulk effects of the radiative heat transfer are non-existent.

According to the criteria defined in Section 3, experimental results on phonic conductivity are presented in Section 4. Compared to similar results available in the literature, they show that the flash technique applied to STM seems to be accurate. The temperature dependence of the phonic conductivity of float glasses and amorphous SiO_2 is found to be in relative agreement with both experimental results obtained by a method in the steady-state regime [10] and theoretical results found using microscopic approaches based on the physics of disordered systems.

2. THE PHYSICAL MODEL AND THE NUMERICAL RESOLUTION

2.1. *Physical model*

A plane-parallel semi-transparent slab of an emitting–absorbing medium is considered. At time $t_0 = 0$, the slab is subjected to a heat pulse on the entire front face. The governing equations of this coupled transfer can be written in one dimension if we assume an azimuthally symmetric radiation. The faces of a frosted glass sample are either coated with a gold substrate (low emissivity), or sprayed with a black paint with high gray emissivity, so that the radiative boundary conditions considered are opaque, diffusely emitting or diffusely reflecting walls. Polished gold-coated surfaces have been considered because decreasing the roughness of the surface leads to a reflectivity increase as long as the roughness stays small compared with the wavelength of the incident radiation even at temperatures close to 800 K. Furthermore use of gold ensures an emissivity that remains independent of both wavelength and temperature. It has been shown experimentally that the diffusivity values obtained for temperatures above 650 K are slightly smaller than

those obtained in the case of frosted surfaces, thus showing that the radiative flux leaving the surfaces has been reduced at the very least. Heat transfer in the sample is only due to bulk effects. The case of specular reflecting boundaries has not been treated yet but would not modify the results in this special case of parallel walls with a lateral surface also being gold coated.

The transient behaviour of temperature within a homogeneous, isotropic slab can be found by solving the energy equation:

$$\rho C_p \frac{\partial T(z,t)}{\partial t} = -\frac{\partial q_c}{\partial z} - \frac{\partial q_r}{\partial z} \quad 0 < z < e \quad t > 0 \qquad (1)$$

where q_c stands for the purely conductive flux $-k_{ph}(\partial T(z,t)/\partial z)$ and q_r for the radiative flux which is responsible for the temperature coupling. The thermal boundary conditions are of the third kind. We introduce a global heat exchange coefficient h to describe the convective–radiative heat losses.

The radiative transfer equation at point $M(z)$ is:

$$\frac{\mu}{\chi_\lambda}\frac{\partial L_\lambda(M)}{\partial z} + L_\lambda(M) = n_\lambda^2 L_\lambda^\circ(T). \qquad (2)$$

Solving this equation with the prescribed boundary conditions allows us to derive the expression of $q_r(M)$ by calculating the analytical expression of:

$$q_r(z) = \int_0^\infty q_{r_\lambda}(z)\,d\lambda = \int_0^\infty \left(2\pi\int_0^1 L_\lambda^+(z,\mu)\mu\,d\mu - 2\pi\int_0^1 L_\lambda^-(z,\mu)\mu\,d\mu\right)d\lambda = \sum_{m=1}^{NB} q_{r_m}(z). \qquad (3)$$

The subscript m stands for a spectral band $\Delta\lambda = [\lambda_1, \lambda_2]$. q_{r_m} is the radiative flux that corresponds to the wavelength band from λ_1 to λ_2.

Classical dimensionless parameters have been used for the thermal problem. Those linked to the radiative formulation are written for each spectral band m. The physical parameters n and χ are mean values calculated on each band, either arithmetically (n_a, χ_a), or, for the absorption coefficient, by using the Rosseland mean absorption coefficient χ_R and the Planck mean absorption coefficient χ_P, defined as follows:

$$\frac{1}{\chi_R} = \frac{\int_{\Delta\lambda}\frac{1}{\chi_\lambda}\frac{dL_\lambda^\circ(T)}{dT}d\lambda}{\int_0^\infty \frac{dL_\lambda^\circ(T)}{dT}d\lambda} \qquad \chi_P = \frac{\int_{\Delta\lambda}\chi_\lambda L_\lambda^\circ(T)\,d\lambda}{\int_0^\infty L_\lambda^\circ(T)\,d\lambda}.$$

χ_P appears as a mean value, weighted by the local bulk emission of the blackbody, and χ_R as a mean value weighted by the local blackbody emission gradient. The derivation of these coefficients and their conditions of application can be found in [11].

Thus the mean or equivalent optical thickness $\tau_{0m} = \chi_m . e$ that enters in the calculations is defined by a spectral band model that uses either χ_a, χ_P or χ_R. In this representation, the opacity coefficient χ_m is a constant, independent of the physical conditions at point M. The same applies to the Planck number expressed by:

$$N_m = \frac{k_{ph}\chi_m}{4n_m^2\sigma T_0^3}.$$

The dimensionless gray radiative flux and intensity are written, respectively:

$$q_{r_m}^* = \frac{q_{r_m}}{4n_m^2\sigma T_0^4} \quad \text{and} \quad L_m^* = \frac{\pi L_m}{4n_m^2\sigma T_0^4}.$$

L_m is simply defined as

$$\int_{\lambda_1}^{\lambda_2} L_\lambda(z)\,d\lambda.$$

It is not a mean intensity, but rather a 'group' intensity as interpreted by Patch [12]. The integrated intensity L is obtained by integrating L_m over each spectral band. This method has already been used by Grant [13] for rationalizing the choice of group constants in non-gray calculations using a variational principle.

In dimensionless form, the energy and radiative flux equations, (1) and (3), become respectively:

$$\frac{\partial\theta^*}{\partial t^*} = \frac{\partial}{\partial z^*}\left(k^*(\theta^*)\frac{\partial\theta^*}{\partial z^*}\right) + S(\theta^*)$$

$$0 < z^* = z/e < 1 \quad t^* > 0 \qquad (4)$$

where

$$S(\theta^*) = -\frac{\partial}{\partial z^*}\left(\sum_{m=1}^{NB}\frac{\tau_{0m}T_0^*}{N_m}q_{r_m}^*(z^*)\right)$$

$$q_{r_m}^*(z^*) = 2L_m^{*+}(0)E_3(\tau_{0m}z^*) - 2L_m^{*-}(1)E_3(\tau_{0m}(1-z^*)) + \frac{\tau_{0m}}{2}\left[\int_0^{z^*}\left(\frac{\theta^*(z'^*)}{T_0^*}+1\right)^4 \times F_{\lambda_1 T(z'^*)-\lambda_2 T(z'^*)}E_2(\tau_{0m}(z^*-z'^*))\,dz'^* - \int_{z^*}^1\left(\frac{\theta^*(z'^*)}{T_0^*}+1\right)^4 \times F_{\lambda_1 T(z'^*)-\lambda_2 T(z'^*)}E_2(\tau_{0m}(z'^*-z^*))\,dz'^*\right]. \qquad (5)$$

The radiative boundary conditions give the expression of $L_m^{*+}(0)$ and $L_m^{*-}(1)$ reported in the Appendix. The term $F_{\lambda_1 T(z'^*)-\lambda_2 T(z'^*)}$ appearing in the integral of relation (5) stands for the fractional blackbody emissive power in the wavelength-temperature band $[\lambda_1 T, \lambda_2 T]$. It is calculated using the polynomial approximations of $F_{0-\lambda T}$ given by Wiebelt [14]. The exponential integrals are calculated with recurrence relationships from the polynomial and rational approximations of $E_1(x)$. The integral is evaluated

numerically using the method of Gaussian quadratures.

The thermal boundary conditions in $z^* = 0$ and $z^* = 1$ are:

$$k^*(\theta^*)\frac{\partial\theta^*}{\partial z^*} = Bi_1 \cdot \theta^* + \sum_{m=1}^{NB} \frac{\tau_{0m} T_0^*}{N_m} q_{r_m}^*(0)$$

$$k^*(\theta^*)\frac{\partial\theta^*}{\partial z^*} = -Bi_2 \cdot \theta^* + \sum_{m=1}^{NB} \frac{\tau_{0m} T_0^*}{N_m} q_{r_m}^*(1).$$

2.2. *Numerical treatment*

The mathematical problem consists of solving a non-linear parabolic equation with a source term (equation (4)) rewritten for simplicity in the following way:

$$\frac{\partial T(z,t)}{\partial t} = -\frac{\partial}{\partial z}\left(p(z,t)\frac{\partial T}{\partial z}\right) - s(z,t,T)$$

$$0 < z < e \quad t > 0. \quad (6)$$

Because of the strong non-linearity of this problem, especially for short times, a fully implicit scheme cannot be used because of the divergence of the calculations at the beginning of the simulation. Thus, a Crank–Nicolson-type method, reported in [15] and known to be more accurate, was used for the calculations. The Crank–Nicolson method consists of evaluating the coefficients at point $(i, n+\frac{1}{2})$ and averaging the values of T at times n and $n+1$ in the evaluation of T and its derivatives. In order to avoid evaluating $T_i^{n+1/2}$, p and s are expanded in a Taylor series about the point $(i, n+\frac{1}{2}, T_i^{n+1/2})$. This led to the following discretized energy equation:

$$\frac{T_i^{n+1,m} - T_i^n}{\Delta t} = D_-\left(p_{i+1/2}^{n+1/2} D_+\left(\frac{T_i^{n+1,m} + T_i^n}{2}\right)\right) - \frac{1}{2}(s_i^{n+1/2,n+1,m-1} + s_i^{n+1/2,n}) \quad (7)$$

with

—Δt, denoting the time step and Δz, the grid spacing,

—$T_i^{n+1,m}$, the temperature variable approximated at the point $(i, n+1)$ for the mth iteration,

—D_+, the forward difference operator $(D_+ f)_i = f_{i+1} - f_i/\Delta z$,

—D_-, the backward difference operator $(D_- f)_i = f_i - f_{i-1}/\Delta z$,

—$p_{i+1/2}^{n+1/2} = \frac{1}{2}(p_{i+1}^{n+1/2} + p_i^{n+1/2})$,

—$s_i^{n+1/2,n+1,m-1} = s(i, n+1/2, T_i^{n+1,m-1})$, the source term evaluated at the point $(i, n+1/2)$ with the values of T evaluated at time $n+1$ at the previous iteration $m-1$.

This method is consistent, and accurate to second order in time and space. Douglas [16] has proved that the solution of equation (7) converges in the $l2$-norm to the solution of equation (4). The only restriction is that $\Delta t/\Delta z$ remains constant which increases the required computation time, as smaller time steps are needed at short times.

Equation (7) leads to a set of linear equations. The problem is solved iteratively with a convenient procedure proposed by Patankar [17].

There are three other specific characteristics of the model.

—The temporal boundary condition is expressed by converting the heat pulse into a temperature jump for the first half-elementary volume of the medium. Thus $\theta^*(0,0) = T^* - T_0^* = 2NM$, with NM being the number of elementary volumes. When the steady-state is obtained, all the volumes have a temperature level equal to one, assuming no heat losses with the surroundings.

—The divergence of the radiative flux at a node is approximated by the rate of variation of the flux between the two boundaries of each volume.

—The emission terms of equation (5), which depend on temperature to the fourth power, are linearized according to the procedure proposed by Shen *et al.* [18]. For this, we use the values of temperature at the previous iteration $m-1$:

$$(T^{n+1,m}+1)^4 = T^{n+1,m}(T^{n+1,m-1^3} + 4T^{n+1,m-1^2} + 6T^{n+1,m-1} + 4) + 1.$$

The algorithm has been tested by comparing results yielded by calculations carried out with a source term which is linear in temperature, with the corresponding analytical solution. The precision of the radiative flux calculations were tested and it has been verified that the flux values stayed equal to zero to eight decimal places for a constant temperature field. Thus the calculation of the divergence of the flux is unnecessary for values less than 10^{-7}.

3. EXPERIMENTAL THERMOGRAMS AND SIMULATED RESULTS

In this section, we present results obtained both experimentally and numerically. Experimental thermograms point out the influence of the radiative boundary limits (black or reflecting) and of the optical thickness of the sample. A great number of simulations have been carried out in the gray case to test the influence of the significant parameters. A large variety of thermograms have been obtained, and the explanation of how their shape is affected by one or another parameter is discussed in [19]. From these thermograms, an apparent diffusivity has been identified. In what follows, the evolution of the difference between the apparent diffusivity and the phonic diffusivity as a function of the thickness of the sample will be discussed (for a given temperature and a given gray absorption coefficient), and the conditions that ensure an experimental measurement of the true phonic conductivity are deduced.

Finally, it is shown that, under operating conditions

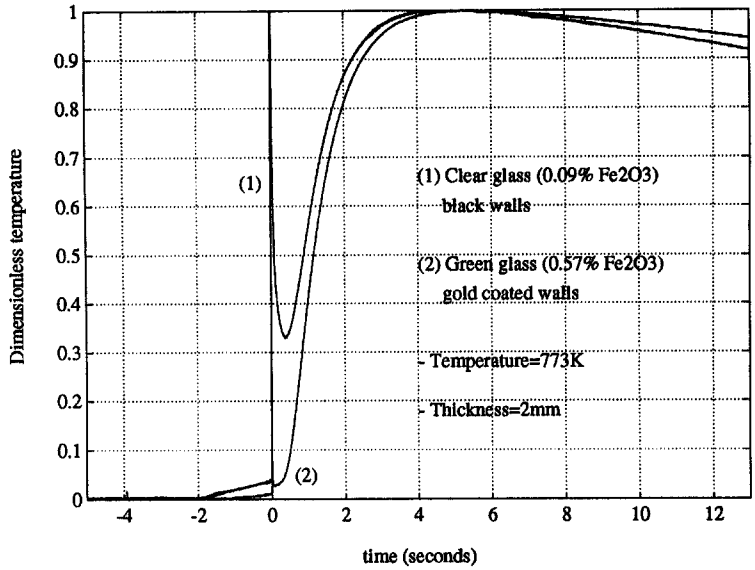

Fig. 1. Experimental rear-face thermograms—influence of the radiative limits.

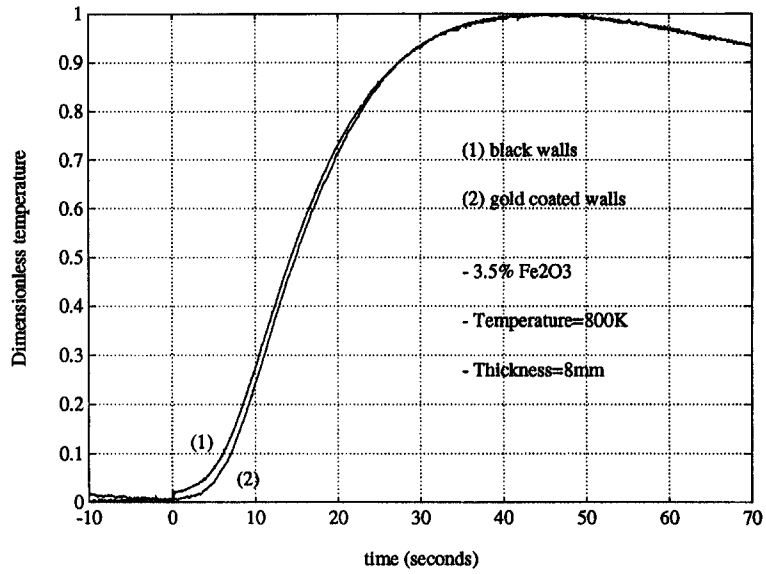

Fig. 2. Experimental rear-face thermograms for a sample of strong optical thickness.

that eliminate the radiative contribution to heat transfer, the non-gray character of the glass does not modify our conclusions. This is illustrated by comparing numerical results obtained with a gray absorption coefficient, with those obtained for a five-band spectral model.

3.1.

Thermograms obtained by an experimental set-up described in [20], are shown in Figs. 1 and 2 and illustrate the difficulty of identifying a diffusivity by such a method. Curve 1 of Fig. 1 shows that, for a clear glass with black walls, the thermal response differs largely from the case of an opaque material. An initial peak appears at very short times. It is caused by a direct exchange between the two black boundaries through a medium of small radiative resistance. The rear face behaves as if it were the perturbed surface. The temperature decreases, passes through a minimum and increases under the progressive influence of a heat flux connected to the coupled mechanism of both conductive and radiative transfer. Such thermograms have been reproduced by numerical simulations. With the exception of the proposal of Tan Heping [21], which came from a numerical study reported in [9], no method is available to find the thermal diffusivity in the case of black radiative limits. If the sample's faces have been previously coated with

a film of evaporated gold (reflecting walls), we obtain a 'classical' thermogram (curve 2). The temperature of the rear face increases continuously from time $t_0 = 0$ (time of the heat pulse) to a maximum, and is a function of the input energy and the heat losses. The thermal response is similar to that of an opaque material, and it is therefore possible to use a high-performance identification process, such as the one based on the partial time moments [22], to identify a diffusivity. The problem is still to determine whether or not the identified parameter is an apparent one (including the radiative transport phenomenon), or representative of the true phonic conduction. To illustrate why it is important to know exactly what is measured in the case of a coupled transfer, we present thermograms (Fig. 2) obtained for a float glass of high Fe_2O_3 content (the colouring agent) and of large thickness (strong optical thickness). The influence of the radiative limits can no longer be distinguished, even at high temperature. One could thus imagine that there are no radiative effects, and that the diffusivity identified in this experiment from the two thermograms is then the correct value of the phonic diffusivity. This is, however, not true in precisely this case since the measured parameter still contains a non-negligible contribution of radiative origin.

3.2. *Influence of the thickness on the identified diffusivity (gray media)*

The influence of the sample thickness of different glasses (different gray absorption coefficient), was also examined. Simulations were carried out for high temperatures in order to amplify radiative effects. The two conditions of perfectly reflecting and perfectly black walls are considered. As the heat exchange coefficients have been set equal to zero, a diffusivity is identified by use of an appropriate partial time from the numerically obtained thermograms. Figure 3 presents the evolution of the apparent conductivity as a function of the slab thickness.

Because of the use of dimensionless variables, the identified parameter represents the value of a conductivity (diffusivity) which is equal to 1 in the purely conductive case and greater than 1 when radiative effects contribute to an enhanced heat transfer. Our results (points of curves 6 and 7) are compared with models of radiative conductivity based on two different approaches:

—the Poltz/Jugel model developed for conductivity measurements in liquids [23] and assuming strong optical thicknesses (curves 1,3),

—the conductivity derived by assuming radiative equilibrium in the medium (curves 2,4).

Figures 3 and 4 show the effect of the thickness on the efficiency of the heat transfer for two values of the Planck number, $N = 2$ and $N = 0.125$, respectively. Curves (1,2,3) are obtained with the two models quoted above. They are limited by values of conductivity, which are independent of the thickness and are given for the upper limit by the Rosseland conductivity (curve 5), and for the lower limit by the phonic conductivity or the conductivity obtained in the case of radiative equilibrium and perfectly reflecting walls (curve 4).

The main conclusion drawn from the analysis of these curves is that the flash method leads to the direct measurement of the phonic diffusivity. However, this measurement is direct only if the thickness of the sample and the boundary conditions are chosen in an appropriate manner. It is noticeable that reflecting walls delay the effect of the thickness on the measured conductivity. This measurement can also be performed by correcting the value of the parameter with the Poltz/Jugel model of radiative conductivity, as this latter seems to correctly describe the rate of heat transfer in the transient regime.

Figure 4 shows, for example, that if one wishes to identify the phonic diffusivity of a glass whose equivalent absorption coefficient is of the order of 15 m^{-1}, the thickness of the sample must be less than 10 mm. Generally speaking, the following criterion should be satisfied: for a STM sample having reflecting surfaces and an equivalent optical thickness (see Section 3.3) less than or equal to 0.1, the flash method will lead to the direct measurement of its phonic diffusivity. In other words, it is possible to define operating conditions for which the flash experiment creates a type of heat transfer that is free from a radiative contribution.

It is also possible, when the optical thickness of the sample is strong enough ($\tau_0 > 10$) so that radiative effects are maximum, to obtain the value of phonic origin by retrieving a conductivity calculated by the simple model of Rosseland.

The last comment concerns the magnitude of the variation of the difference between the phonic and apparent conductivities. The more efficient the radiative transfer is (low values of N), the more important this difference will be. This can be seen in Fig. 4, where the gray-tinted rectangle represents the frame of Fig. 3. If the material is transparent, it will be easier to respect the criterion regarding the sample's thickness. But the slightest departure over this limit rapidly leads to a large error if measurement of this parameter is taken as a phonic conductivity measurement.

It is not necessary to discuss the effect of the temperature as it is evident that lowering the temperature of the experiment reduces the radiative effects caused by emission of the medium.

3.3. *The non-gray medium*

The previous result, confirmed by experimental measurements of the phonic diffusivity of glasses and presented in Section 4, supposes that we can affect an equivalent absorption coefficient to a glass over the whole thermal spectra. From a physical point of view, it is to be expected that in conditions that eliminate the radiative contribution to heat transfer (no bulk

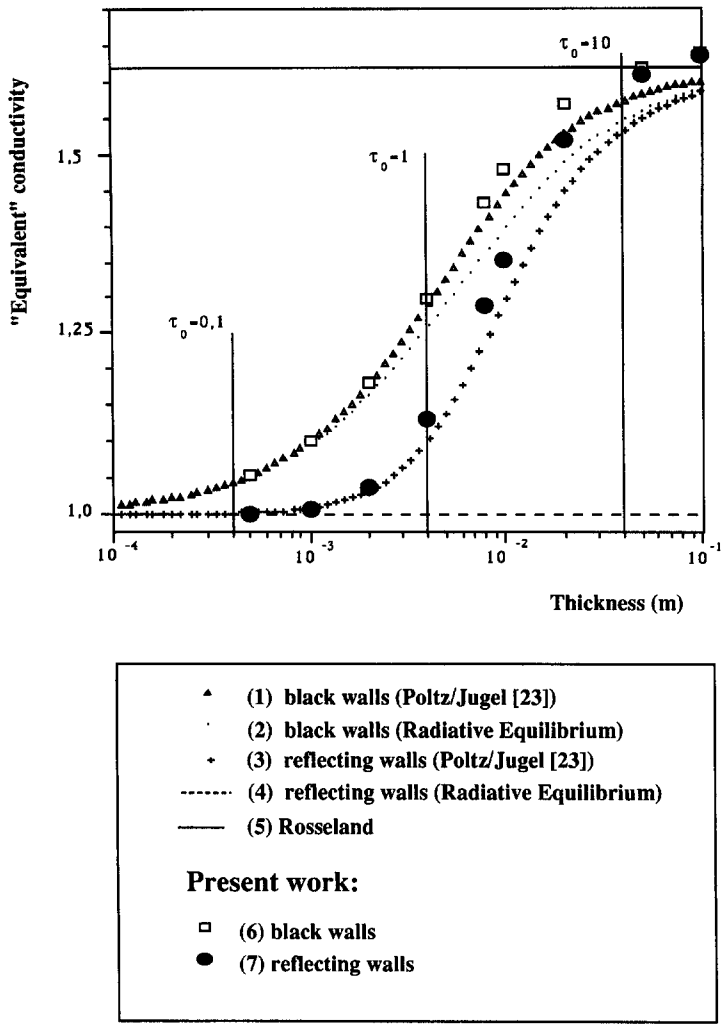

Fig. 3. Influence of the thickness on the apparent diffusivity (T_0 = 800 K, χ = 250 m^{-1}, N = 2).

effects in the sample), the non-gray character of a glass does not play any role. This section is devoted to the verification of this point in order to consider possible explanations for the errors resulting from the hypothesis of a gray medium. The spectral dependence of the refractive index is not considered here. The mean gray absorption coefficients of Planck and Rosseland, and the mean band coefficients are calculated from the absorption spectra of various float glasses measured by Banner [24] at St-Gobain Recherche Company, using the definition of χ_a, χ_P, χ_R.

Figure 5 gives the absorption spectra at 773 K of the clearest of these float glasses (0.09% Fe_2O_3) and the multi-band models that will be used in the simulations. Table 1 shows an example of the numerical values of the mean band coefficients. The gray-equivalent coefficients calculated by χ_R and χ_P are also shown. We have considered a sample thickness of 2 mm. Both black and reflecting walls have been studied. In the case of reflecting walls (Fig. 6), the non-gray model lead to thermograms that do not differ from those obtained with the mean gray coefficients. The use of one or the other coefficient for the band model has no appreciable influence on the solution. By analysing the partial times $t^*_{1/2}$ in each case (Table 2) and comparing the values to 0.139, the value of the purely conductive case, it can be seen that the errors of radiative origin do not exceed 3%. Table 3 shows that the relative discrepancies between the gray medium and the band-gray medium are moderate and less than 1% when the spectra is represented by the Rosseland equivalent coefficient. It can also be seen that the use of χ_R better fits the multi-band description defined using the Rosseland mean coefficient (0.75%), than is the case using coefficients defined by the Planck mean (1.16%). It is therefore recommended that an equivalent gray coefficient be calculated using χ_R in order to determine the maximum thickness that can be considered in order to ensure direct measurement of the phonic diffusivity. For example, when χ_R = 141.5 m^{-1} for the clearest glass, and for a thickness of 2 mm, an optical thickness

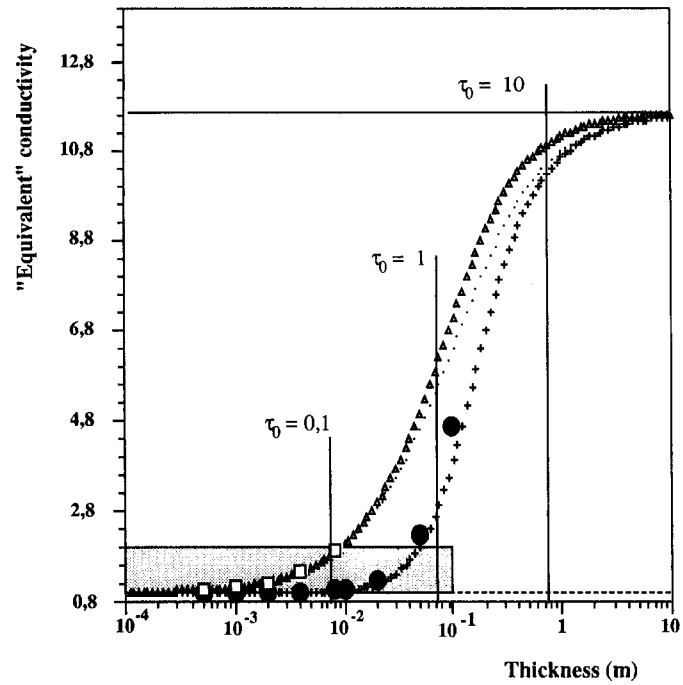

Fig. 4. Influence of the thickness on the apparent diffusivity ($T_0 = 800$ K, $\chi = 15$ m^{-1}, $N = 0.125$).

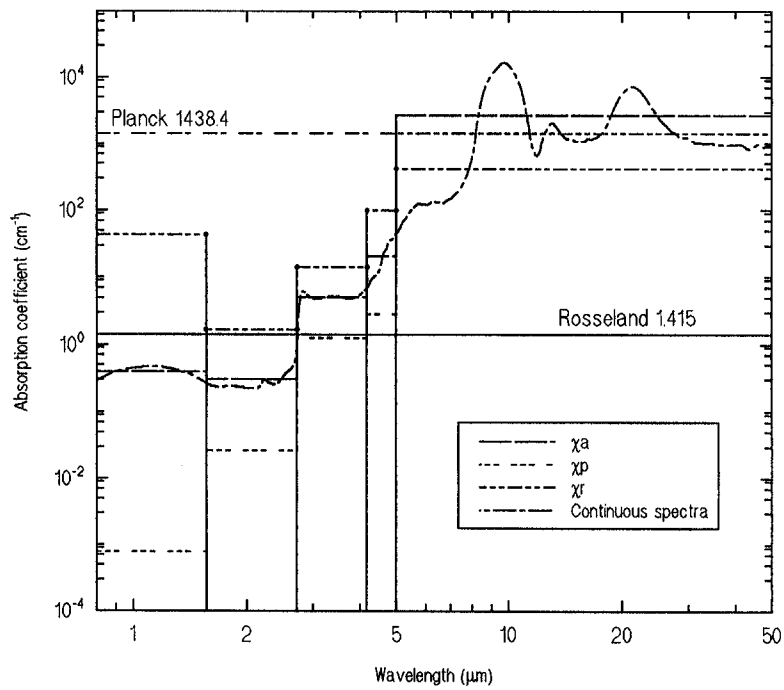

Fig. 5. Absorption coefficient of a clear float glass and its associated five-band models.

of 0.28 is obtained. Looking back at Figs. 3 and 4 shows that this is a moderate case, and that the true conductivity will undoubtly be measured. Here, the error due to radiation is so small that it cannot be differentiated from the experimental error.

In the case of black walls, the non-gray character of the glass modifies the pulse thermal response at short times. The use of one or another mean coefficient in the band model is important. This can be seen in Fig. 7, especially for small times. The curves labelled (3) represent the non-gray case with the band values of the absorption coefficient calculated using the

Table 1. Band model of the absorption coefficient of a clear float glass at 773 K

$\lambda_k - \lambda_{k+1}$	χ_R (cm^{-1}) Rosseland	χ_P (cm^{-1}) Planck	χ_a (cm^{-1}) arithmetic
0.8–1.56	43.52	0.00078	0.391
1.56–2.72	1.66	0.0267	0.301
2.72–4.18	14.12	1.247	5.087
4.18–5.05	99.33	2.816	20.72
5.05–54.94	414.42	1434.37	2665.8
Gray	1.415	1438.4	1438.46

Table 2. Relative errors between the diffusivities obtained by simulation in the gray and non-gray case and the phonic diffusivity (reflecting walls)

Simulation cases	Time $t^*_{1/2}$	Error (%)
5 bands χ_P	0.136 05	2.12
5 bands χ_a	0.1353	2.66
5 bands χ_R	0.134 92	2.93
Gray χ_R	0.135 95	2.19
Gray χ_P	0.137 65	0.97
Phonic conductivity	0.139	0

Rosseland, Planck or arithmetic mean. With χ_a, the thermal response is halfway between the faster, obtained with χ_P (dotted line), and the slower one, obtained with χ_R. The curves obtained using either χ_P or χ_R as gray equivalent coefficient for the whole spectra can differ significantly. The use of χ_P in a multiband model or χ_R in the gray equivalent model agrees well with experimental results. This has been confirmed by simulations of 10 spectral bands (on the other hand, the change from a 5-band model to a 10-band model does not change the thermal response obtained with reflecting walls).

Table 3. Relative errors in (%) between the diffusivities obtained in the gray case and the non-gray case (reflecting walls)

Non-gray band coefficients	Gray	
	χ_R	χ_P
χ_R	0.75	1.98
χ_a	0.5	−1.7
χ_P	−0.07	1.16

This example shows that the absorption spectra must be precisely known for the identification from a global measurement of a parameter of purely phonic origin. This is precisely the problem that limits the use of the hot-wire technique for such a measurement.

4. EXPERIMENTAL RESULTS FOR PHONIC CONDUCTIVITY

We present results of phonic conductivity for a silica glass since this medium is a reference. Our experimental study on float glasses of various Fe_2O_3 content can be found in [25]. Figure 8 presents only one result obtained on the clearest float glass (0.09% Fe_2O_3) and the most reliable data found on the same glass (0.042% Fe_2O_3). The discrepancies between the conductivity values at a given temperature may be due to the characteristics of each experimental set-up. But the agreement is good (2.5% of difference between the slope values) in terms of the temperature dependence of k_{ph}.

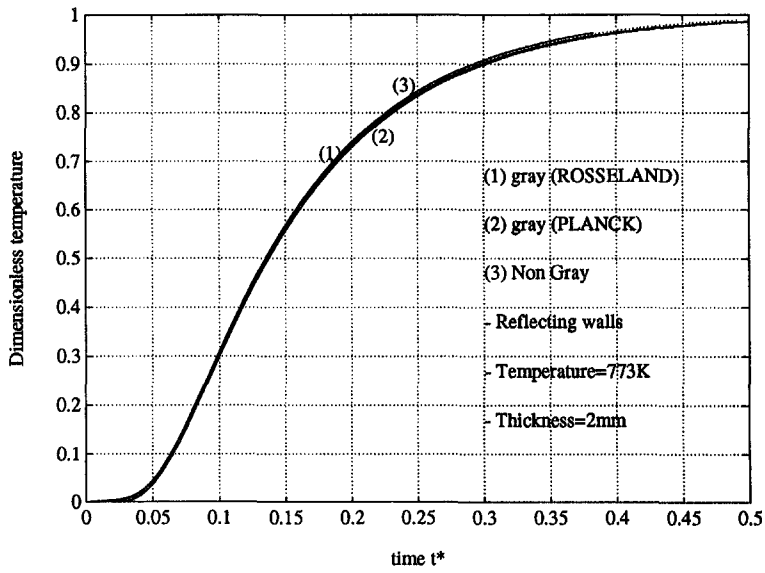

Fig. 6. Experimental rear-face thermograms in the gray and non-gray case for a clear glass having reflecting boundaries.

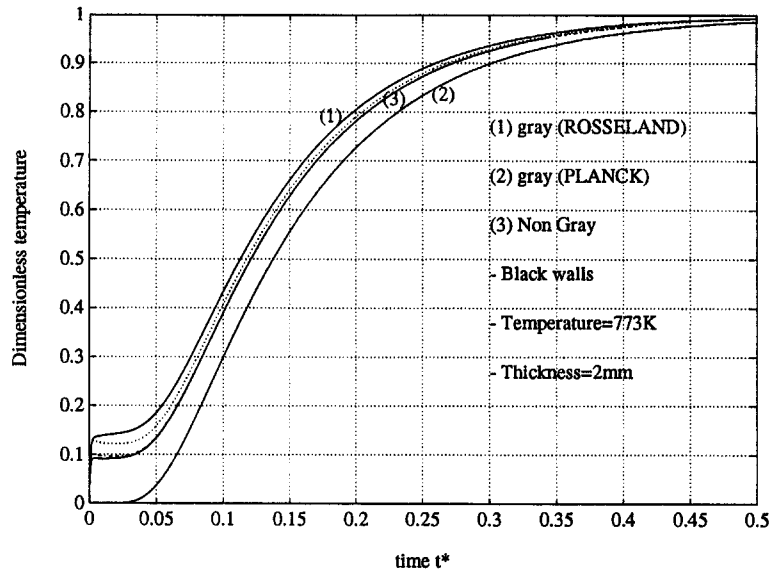

Fig. 7. Experimental rear-face thermograms in the gray and non-gray case for a clear glass having black boundaries.

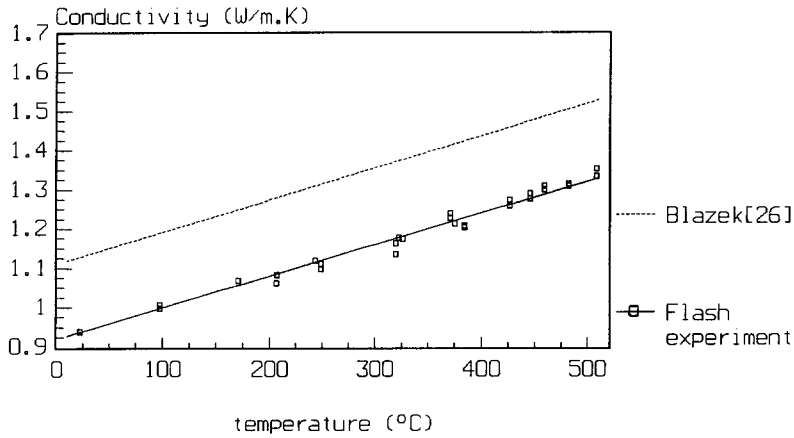

Fig. 8. Phonic conductivity of a clear float glass (0.09% Fe_2O_3) vs temperature.

The gray mean absorption coefficient χ_R can be calculated from the absorption spectra of silica. A sample of 2 mm thickness has been tested in order to satisfy the criterion of optical thickness inferior to 0.1. The sample was coated with gold in order to obtain reflecting walls. Simulations have shown that a total reflectivity of 90–100% does not significantly affect the value of the identified parameter. The corresponding values of thermal conductivity were derived from the thermal diffusivity measurements, using Richet's results for $C_p(T)$ [26]:

$$C_p(T) = 0.917 + 0.3 \times 10^{-3} T - 25140/T^2 \ (\mathrm{J\,g^{-1}K^{-1}}).$$

The density ρ is equal to 2.2 kg m^{-3} (the variation between 300 and 800 K is less than 0.1%).

Figure 9 presents the evolution of the phonic conductivity of SiO_2 vs temperature. The dashed curve fits the data according to the following relation:

$$k_{ph1}(T) = 1.18 + 3.14 \times 10^{-3} T - 17966/T^2 \ (\mathrm{W\,m^{-1}K^{-1}}).$$

This result confirms that, as predicted by microscopic approaches in solid-state physics, the temperature dependance of k_{ph} is similar to that of the specific heat.

Other published experimental results on SiO_2 report a linear dependence of k_{ph} on temperature. This may prove that in those experiments a radiative contribution to k_{ph} exists (either due to the experimental set-up or to the model used in the identification pro-

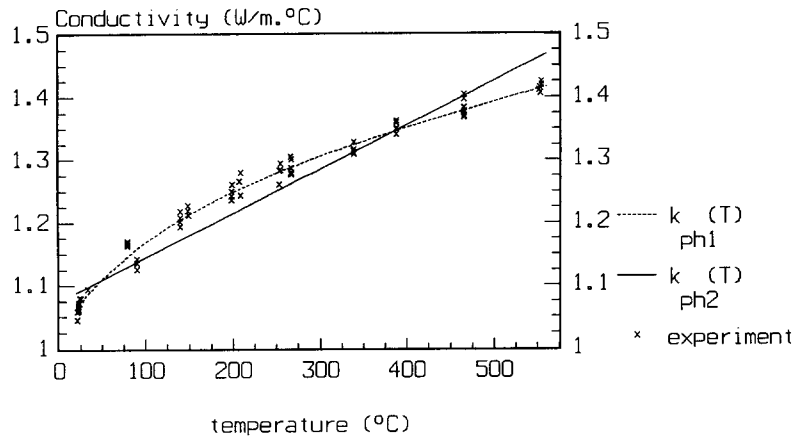

Fig. 9. Phonic conductivity of silica glass (Puropsil quality, thickness = 2 mm, polished gold-coated surfaces).

cess), which is greater than the uncertainty on the measurement. The concavity of the curve shows that even at high temperatures, k_{ph} tends not to increase but rather to remain at a relatively stable value until the glass transition point.

Despite this, a linear regression applied to our experimental results (solid line of Fig. 9) gives:

$$k_{ph2} = 1.075 + 7.05 \times 10^{-4} T (\mathrm{W\,m^{-1}\,K^{-1}})$$

Compared with the results of Kunc [27], the slope coefficient is in good agreement (12% lower) for silica glass and on the same order as the one found for float glasses (70% SiO_2) [25].

5. CONCLUSION

In order to show that the flash method applied to STMs can lead to the measurement of the true thermal diffusivity, a theoretical model of the 1D transient coupled heat transfer has been developed, and the numerical treatment of the problem solution has been detailed. Due to extremely high computation times, the use of the model in an identification process has not been considered, but simulations have shown that, for conditions of small equivalent optical thickness and in the case of reflecting walls, the flash method provides a direct measurement of the phonic diffusivity of glasses in the same way as it does for opaque materials. In Section 3, it was shown that the spectral dependence of the absorption coefficient can be taken into account only through the knowledge of the Rosseland mean coefficient.

Finally, experimental results for the thermal conductivity of SiO_2 are presented. A new expression for the phonic conductivity was derived. It was used to confirm that the flash technique is well-adapted to the characterization of STMs, since operating conditions can be found in order to avoid any radiative contribution to heat transfer. Furthermore, our results confirm microscopic theoretical models of the conductivity of disordered systems.

REFERENCES

1. K. Prasad and R. J. Hering, Transient radiative heat transfer in a plane layer, *Int. J. Heat Mass Transfer* **12,** 1331–1337 (1969).
2. A. S. Hazzah and J. V. Beck, Unsteady combined conduction-radiation energy transfer using a rigorous differential method, *Int. J. Heat Mass Transfer* **13,** 517–522 (1970).
3. C. C. LII and M. N. Özisik, Transient radiation and conduction in an absorbing, emitting, scattering slab with reflective boundaries, *Int. J. Heat Mass Transfer* **15,** 1175–1179 (1972).
4. D. G. Doornink and R. G. Hering, Transient combined conductive and radiative heat transfer, *J. Heat Transfer* **94,** 473–478 (1972).
5. R. Viskanta and E. E. Anderson, Heat transfer in semi-transparent solids, *Adv. Heat Transfer* **11,** 317–441 (1975).
6. J. B. Saulnier, La modélisation thermique et ses applications aux transferts couplés et au contrôle actif, Thèse de Doctorat d'Etat, Université de Poitiers (1980).
7. H. C. Hottel and A. F. Sarofim, *Radiative Transfer.* McGraw-Hill, New York (1967).
8. Tan Heping and M. Lallemand, Transient radiative-conductive heat transfer in flat glasses submitted to temperature, flux and mixed boundary conditions, *Int. J. Heat Mass Transfer* **32,** 795–810 (1989).
9. Tan Heping, B. Maestre and M. Lallemand, Transient and steady-state combined heat transfer in semi-transparent materials subjected to a pulse or a step irradiation, *J. Heat Transfer* **113,** 166–173 (1991).
10. T. Kunc, M. Lallemand and J. B. Saulnier, Some new developments on coupled radiative-conductive heat transfer in glasses—experiments and modelling, *Int. J. Heat Mass Transfer* **27,** 2307–2319 (1984).
11. H. S. Douglas, Choice of an appropriate mean absorption coefficient for use in the general grey gas equations, *J. Quant. Spectrosc. Radiat. Transfer* **5,** 211–225 (1965).
12. R. W. Patch, Effective absorption coefficients for radiant energy transport in nongrey, nonscattering gases, *J. Quant. Spectrosc. Radiat. Transfer* **7,** 611–635 (1967).
13. I. P. Grant, On the representation of frequency dependence in non-grey radiative transfer, *J. Quant. Spectrosc. Radiat. Transfer* **5,** 227–243 (1965).
14. J. A. Wiebelt, *Engineering Radiation Heat Transfer,* Holt, Rinehart and Winston, New York (1966).
15. G. A. Sod, *Numerical Methods in Fluid Dynamics,* pp. 116–142. Cambridge University Press Cambridge (1985).
16. J. Douglas Jr, The application of stability analysis in the

numerical solution of quasi-linear parabolic differential equations, *Trans. Am. Math. Soc.* **89,** 484 (1958).
17. S. V. Patankar, *Numerical Heat Transfer and Fluid Flow*. Hemisphere, New York (1980).
18. Z. F. Shen, T. F. Smith and Penelop Hu, Linearization of the radiations terms for improved convergence by use of the zone method, *Numer. Heat Transfer* **6,** 377–382 (1983).
19. S. Andre and A. Degiovanni, The flash method applied to semi-transparent materials: 'apparent' diffusivity or 'phonic' diffusivity? *Proceedings of EUROTHERM Sem.no.*21, *Editions Européennes Thermique Industrie*, pp. 249–258 (1992).
20. S. Andre and A. Degiovanni, An extension of the flash technique in the 300 K to 800 K temperature range: application to thermal diffusivity measurement of semi-transparent materials. *Heat Transfer* 2, *IChemE Symposium Series*, pp. 1197–1203 (1992).
21. Tan Heping, Problème inverse du transfert couplé pour la détermination de la conductivité thermique des matériaux semi-transparents. *J. Aerospace Power*, **6,** 275–278 (1991).
22. A. Degiovanni and M. Laurent, Une Nouvelle Technique d'Identification de la Diffusivité Thermique pour la Méthode Flash. *Rev. Phys. Appl.* **21,** 229–237 (1986).
23. H. Poltz and R. Jugel, The thermal conductivity of liquids IV/: temperature dependence of thermal conductivity, *Int. J. Heat Mass Transfer* **10,** 1075–1088 (1967).
24. D. Banner, Propriétés radiatives des verres et des fontes de silicates en fonction de la température. Modélisation des transferts thermiques. Thèse de Doctorat de l'Ecole Centrale de Paris (1991).
25. S. Andre and A. Degiovanni, Experimental measurements of the phonic diffusivity of semi-transparent materials up to 800 K. *Glas. Ber.* **66,** 1–8 (1993).
26. A. Blazek, Review of thermal conductivity data of glass. Compiled by Technical Committees of the International Commission on Glass. *Institut National du Verre*, Charleroi, Belgique (1983).
27. T. Kunc, Etude du transfert couplé conduction-rayonnement. Application à la détermination de la conductivité phonique des verres à haute température par identification paramétrique. Thèse de 3ème cycle, Université de Poitiers (1984).

APPENDIX

$$L_m^{*+}(0) = \frac{a_{1m}^* + b_{1m}^* a_{2m}^*}{1 - b_{1m}^* b_{2m}^*}$$

$$L_m^{*-}(1) = \frac{a_{2m}^* + b_{2m}^* a_{1m}^*}{1 - b_{1m}^* b_{2m}^*}$$

$$a_{1m}^* = \frac{\varepsilon_{1m}}{4}\left(\frac{\theta_{(0)}^*}{T_0^*} + 1\right)^4 F_{\lambda_1 T(0) - \lambda_2 T(0)}$$

$$+ 2\rho_{1m}\int_0^1 \frac{\tau_{0m}}{4}\left(\frac{\theta^*(z'^*)}{T_0^*} + 1\right)^4 F_{\lambda_1 T(z'^*) - \lambda_2 T(z'^*)} E_2(\tau_{0m} z'^*)\, \mathrm{d}z'^*)$$

$$a_{2m}^* = \frac{\varepsilon_{2m}}{4}\left(\frac{\theta_{(1)}^*}{T_0^*} + 1\right)^4 F_{\lambda_1 T(1) - \lambda_2 T(1)}$$

$$+ 2\rho_{2m}\int_0^1 \frac{\tau_{0m}}{4}\left(\frac{\theta^*(z'^*)}{T_0^*} + 1\right)^4 F_{\lambda_1 T(z'^*) - \lambda_2 T(z'^*)} E_2(\tau_{0m}(1 - z'^*))\, \mathrm{d}z'^*$$

$$b_{im}^* = 2\rho_{im} E_3(\tau_{0m}) \quad \text{for} \quad i = 1, 2.$$